Investigation into the Acoustics and Performance Characteristics of an Ideally Twisted Rotor Using Experiments and Low Fidelity Prediction Tools

Nicole A. Pettingill,* Nikolas S. Zawodny,† Christopher Thurman,‡
Leonard V. Lopes,§
NASA Langley Research Center, Hampton, VA, 23681

A series of experiments were conducted in an anechoic chamber to investigate the noise and performance of an ideally twisted rotor design, leading to validation of a low-fidelity aerodynamic performance and acoustic modeling tool chain. An "ideally twisted" rotor was designed in order to simplify the theoretical rotor inflow for a target thrust condition in hover. This rotor design was then fabricated using state-of-the-art rapid prototyping and tested in an anechoic chamber facility. Aerodynamic load and acoustic data were acquired across a range of rotation rates (RPM) and rotor collective settings in order to ascertain the accuracy of the low-fidelity modeling codes. Emphasis was placed on modeling of the broadband self-noise generated by the rotor system due to the fact that it was found to be a prominent contributor to the overall rotor system noise.

Nomenclature

English

A_0	Rotor collective angle, deg.
c	Chord length, m
C_T	Thrust coefficient, $\frac{T}{\rho\pi\Omega^2 R^4}$
M_{tip}	Tip Mach number
N_b	Number of rotor blades
Q	Torque, N $\cdot$ m
r	Spanwise location from hub, m
R	Blade radius, m
St	Strouhal number rel. to chord, $\frac{fc}{U_{tip}}$
T	Thrust, N
U_{tip}	Tip Speed, m/s

Greek

α	Local aerodynamic angle of attack, deg.
ϕ	Local induced angle, deg.
σ	Rotor solidity, $\frac{N_b c}{\pi R}$
$\theta_\circ$	Observer angle in SHAC, deg.
Θ	Blade pitch angle, deg.
Θ_{tip}	Blade tip pitch angle, deg.
Ω	Rotation rate, RPM

*Research Aerospace Engineer, Aeroacoustics Branch, AIAA Member; nicole.a.pettingill@nasa.gov
†Research Aerospace Engineer, Aeroacoustics Branch, AIAA Member; nikolas.s.zawodny@nasa.gov
‡Research Aerospace Engineer, Aeroacoustics Branch, AIAA Member; christopher.thurman@nasa.gov
§Research Aerospace Engineer, Aeroacoustics Branch, AIAA Member; leonard.v.lopes@nasa.gov

Subscript
c Corrected rotation rate (for sea level, standard day conditions)
max Highest RPM condition
tip Tip condition
$mech$ Mechanical RPM

I. Introduction

Characterizing noise sources in small rotor blades is important as they are applicable to small UAS, and potentially to larger, UAM vehicle platforms. Furthermore, assessment of the available low fidelity tools is important as they will be used to predict noise sources and influence the vehicle design process. This paper will serve in further validation of semi-empirical noise prediction tools. A set of hover chamber experiments and corresponding predictions of an ideally twisted rotor brought about interesting results that will be discussed in this paper. While hover tests for rotors of these scales have been done, they have normally been done with commercial of the shelf (COTS) rotors. With these COTS rotors, it is not always possible to know the exact geometric properties or the complexity of the inflow. A rotor with an ideal twist distribution theoretically has uniform inflow, which may be simpler to predict using low fidelity tools. The predictions of this abstract will be on harmonic content and broadband self-noise, however the final paper will discuss additional noise sources that may have been present in the experiment. The experimental work and predictions in this paper have helped with understanding the current broadband noise prediction method and its limitations. This in turn has influenced the development of the broadband noise prediction module in the ANOPP2[1] design suite. The toolset used for this abstract is PAS, ROTONET, and BARC. A similar broadband prediction methodology has been employed previously published predictions of small rotors, such as in Ref. 2. While broadband noise predictions in this abstract are presented using a semi-empirical tool called Broadband Acoustic Rotor Codes (BARC), the final paper will present these predictions using the ANOPP2 Self Noise Internal Functional Module (ASNIFM).

This abstract will first provide a background in ideally twisted rotors, blade element theory and past experiments and prediction work. Following this, the testing facility will be introduced, and results will be shown, along with preliminary prediction methods. Finally, the status of the work will be discussed along with results that will be discussed in the final paper.

A. Rotor Design

The design parameters and conditions for the rotor in this study are summarized in Table 1. Blade element momentum theory with an ideal twist distribution was used to design the rotor. This method, described in Ref. 3, defines a rotor which experiences uniform inflow and thus minimum induced power in hover. An ideally twisted rotor with a constant chord is defined by the following blade pitch distribution:

$$\Theta(r) = \frac{\Theta_{\text{tip}}}{r}, \tag{1}$$

and the local angle of attack and inflow angles are defined as:

$$\alpha(r) = \frac{\alpha_{\text{tip}}}{r}, \tag{2}$$

$$\phi(r) = \Theta(r) - \alpha(r). \tag{3}$$

Table 1. Ideally twisted rotor design parameters.

	Parameter	Value
Geometry	R (m)	0.1588
	c/R	0.20
	Θ_{tip} (°)	6.9
	N_b	4
	σ	0.255
Operating Condition	C_T	0.0137
	M_{tip}	0.27
	Ω_c (RPM)	5500

The 4-bladed rotor was sized to a radius of R = 0.1588 m. Dimensionally speaking, the rotor was designed to generate 11.12 N (2.5 lbs.) of thrust at a rotational speed of $\Omega_c = 5500$ RPM. The distribution of Θ, α and ϕ along the span can be seen in Fig. 1. Thus, the nominal tip angles were a blade pitch of 6.9 degrees, induced angle of 4.7 degrees, and angle of attack of 2.1 degrees. The resulting thrust coefficient was $C_T = 0.0137$, with a tip Mach number of $M_{\text{tip}} = 0.27$.

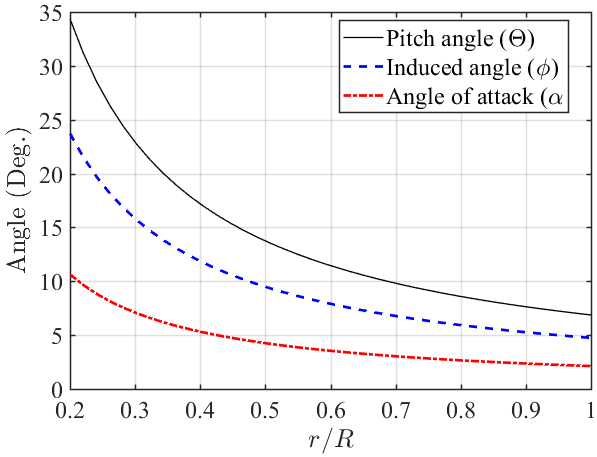

Figure 1. Spanwise angle distributions for designed ideally twisted rotor.

B. Blade Manufacturing

The printing of a tall and thin structure such as a rotor blade was expected to be challenging, and several iterations were expected, which lead to the decision to print these blades in house. The blades were manufactured at the NASA Langley *Larkworks MakerSpace* using a Markforged X7 3D printer. This printer has a build volume of 330 mm x 270 mm x 200 mm, a minimum possible layer height of 50 μm and produces fiber-reinforced plastic parts. The blades tested in this study were printed out of carbon fiber-reinforced onyx plastic. The blades were printed such that layers were printed in the radial direction. The blades were also printed with the blade standing from the leading edge. This layering technique resulted in a smooth airfoil definition in the chordwise direction. The blades were found to be very challenging to print due to a combination of the blade orientation during layering as well as the fact that only one blade could be printed at a time. As Fig. 2(a) shows, the blades were printed with mixed success. However, the blades that did print successfully were of excellent overall build quality and surface finish. The blade roots were designed to mate with a COTS hub made by varioPROP, which is a small-scale ground adjustable variable pitch propeller hub (see Figs. 2(b) and 2(c)). Using this hub it was possible to manually adjust the pitch of all 4 blades simultaneously.

(a) Blade printing iterations

(b) varioPROP hub

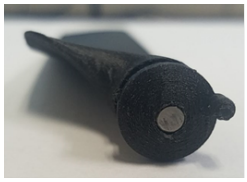

(c) Blade root design

Figure 2. Rotor blade manufacturing.

C. Experimental Setup

The experiment was conducted in the the Small Hover Anechoic Chamber (SHAC), a facility at the NASA Langley Research Center. Photos of the setup are shown in Figure 3. The SHAC is acoustically treated down to 250 Hz and has dimensions of 3.87 x 2.56 x 3.26 m from wedge tip to wedge tip. This facility has been found in recent studies to be suitable for measuring the aerodynamic loads and acoustics of small rotors in static conditions when proper precautions are taken to address and mitigate the effects of flow recirculation (Ref. 4, 5). Two mesh screens are placed in the chamber to reduced recirculation effects, as seen in the schematic in Figure 3(c). More details of recirculation, the mesh setup, and their effect will be discussed in the final paper. A Bruel & Kjaer (B&K) LAN-XI DAQ and BK Connect software system are used for for data acquisition. Six B&K Type 4939 free-field microphones are located in the upper corner of the SHAC, and span a range of $+43.5°$ above the plane of the rotor, to $-43.1°$ below the plane of the rotor. These microphones are located about 12 rotor radii away from the rotor, which is in the far-field. A laser sensor tachometer located directly below the rotor was used to monitor the rotational rate of the rotor , and a 6-component AI-IA mini40 multiaxis load cell was used to measure the loads. The rotor was powered using a Scorpion 4020 DC brushless motor and a Castle Creations Edge 50 electronic speed controller.

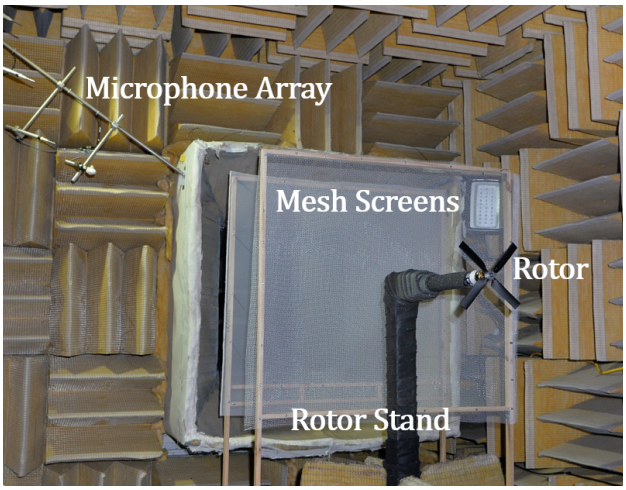

(a) Testing set up in SHAC facility

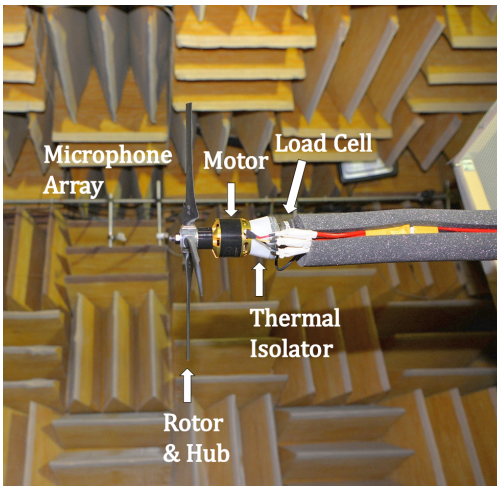

(b) Mounted rotor, motor and load cell

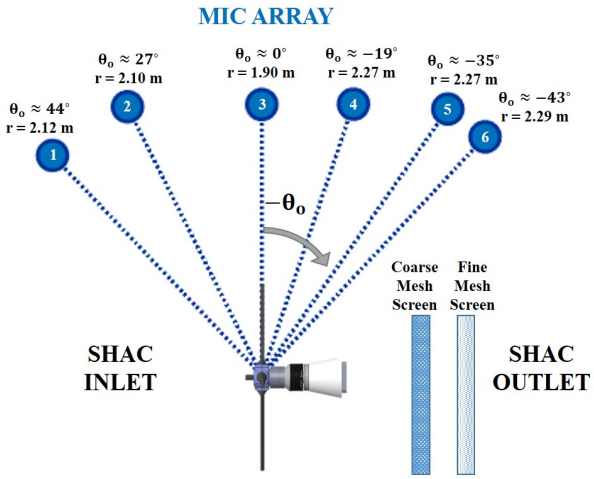

(c) Acoustic measurement layout (not to scale)

Figure 3. SHAC facility and acoustic measurement configuration.

The test cases were divided into two primary parameter sweeps: a rotor rotation rate sweep and a rotor collective sweep. A summary of the testing conditions is provided in Table 2. The sweep of rotor rotation rates were acquired first to establish the target design operating condition, and these were done at the designed blade pitch of $\Theta_{\text{tip}} \approx 6.9°$. Following this, the root pitch was was adjusted with the vario-prop hub to collectives of $A_0 \approx \pm 3°$.

Table 2. Experimental testing conditions.

Parameter Sweep	Ω (RPM)	Θ_{tip} (°)
Rotation Rate (Ω)	3000⇒6000[a] [b]	6.9
Rotor Collective (A_0)	5500[a]	3.9, 6.9, 9.9

[a]Values are approximate.

[b]Tested in approximate increments of 500 RPM.

D. Low Fidelity Prediction Tools

Several low fidelity rotor performance and acoustic prediction tools are utilized in this study. The first two are part of the NASA Aircraft NOise Prediction Program (ANOPP), and are called the Propeller Analysis System (PAS)[6] and the Rotorcraft System Noise Prediction System (ROTONET).[7] These codes utilize blade element momentum theory (BEMT) to predict the aerodynamic loads on respective propellers and rotors. Broadband rotor self-noise predictions are currently performed using the Broadband Acoustic Rotor Codes (BARC) suite.[2,8–10] This suite incorporates the semi-empirical airfoil self-noise prediction routines of Reference 8 into a rotating reference frame, given the appropriate aerodynamic conditions of discrete blade elements.

In this study, PAS is utilized to predict the tonal noise characteristics of the ideally twisted rotor due to the fact that it has a more accurate acoustic solver that accounts for the full pressure distribution on the blade surface, while the current implementation of ROTONET utilizes a compact chord assumption. The ROTONET performance module assumes a fully articulated rotor with rigid blades and a simple uniform inflow model.[11]ROTONET is specifically utilized to compute the inflow characteristics for the rotor in hover conditions, which is a condition that PAS cannot model. An inflow velocity is required as an input into PAS and therefore cannot truly represent a hover condition. However, it has been found that a reasonably accurate prediction of a hover condition can be achieved with only a modest freestream velocity condition.[10] ROTONET uses rotor definitions and flight conditions such as thrust, rotor angle, rotor speed, advance ratio and trim conditions as inputs in order to calculate inflow conditions for BARC.

BARC uses NACA0012 empirical boundary layer data, and thus requires a tripped or untripped boundary layer definition as an input.

II. Preliminary Results

This section will present preliminary results of both performance and acoustic test data.When presenting acoustic spectra in this abstract it, it will be shown from microphone 5, which is located about $-35°$ below the plane of the rotor. Some preliminary tonal and broadband noise predictions will be presented. The final paper will include additional test cases, comparisons to predictions and a more thorough analysis of the noise characteristics of this rotor.

A. Performance Measurements

As described in the experiment section, a sweep of rotation rate conditions was performed for the design blade pitch of $\Theta_{tip} \approx 6.9°$. Following this, the collective was adjusted so that the blade pitch at the tip was $\pm 3°$ from the baseline condition (resulting in a near constant tip speed of about $M_{tip} \approx 0.26$). Table 3 lists the performance measured for these cases as well as the resulting thrust coefficient $C_T = \dfrac{T}{\rho \Omega^2 R^4}$ and tip Mach number M_{tip}.

Table 3. Performance of Ideally Twisted Rotors in SHAC

Pitch	Ω_{mech}	Thrust	$Mtip$	C_T
6.9	5989	13.42	0.2893	0.0141
6.9	5480	10.67	0.2648	0.0133
6.9	5070	8.74	0.2449	0.0128
6.9	4470	6.43	0.2159	0.0121
6.9	4010	4.96	0.1937	0.0116
6.9	3375	3.38	0.1630	0.0112
6.9	2963	2.47	0.1431	0.0106
3.9	5465	6.38	0.2638	0.0080
6.9	5480	10.67	0.2648	0.0133
9.9	5514	14.46	0.2633	0.0179

Thrust was plotted against rotational rate (corrected for standard day conditions) in Figure 4(a). A second-order fit was applied to the RPM sweep, and the designed target thrust of 11.12 N fell on the line, indicating the ideal rotor is performing as predicted. The torque was also plotted against rotational rate in Figure 4(b) and also followed a second-order curve fit. The two pitch collective cases are also plotted in both curves, to show they were targeted at the baseline rotation rate of $\Omega_c \approx 5400 RPM$.

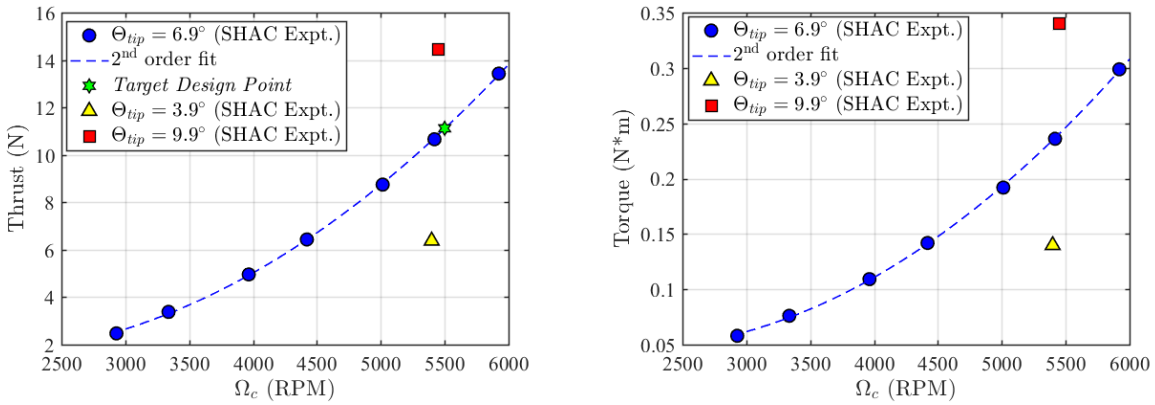

(a) Thrust vs RPM

(b) Thrust vs Torque

Figure 4. Thrust and torque were plotted against corrected RPM in for both the RPM sweep and pitch results.

B. Processing the Acoustic Data

The following steps were taken to extract the broadband, nonperiodic content from the raw data (for additional information on the data processing techniques see Ref. 12). First, the narrowband acoustic spectra were computed using by using a fast Fourier Transform (FFT) from raw data treated as random data sets. This raw spectra is plotted in Figure 5(a). Second, to separate the periodic and random components, the mean rotor revolution time history was computed. This was then subtracted from the time record to retain random noise components. An FFT was used to compute the periodic and broadband spectra from these mean and residual time series, and both spectra are plotted in Figure 5(b). Finally, remaining peaks left in the residual signal were removed to more clearly see the broadband component. This "peak-removed" can be seen in black in Figure 5(c). This final result spectra is used for comparison with predictions, though it should be noted that the peak removal technique may not always be effect as it sometimes removes broadband noise content.

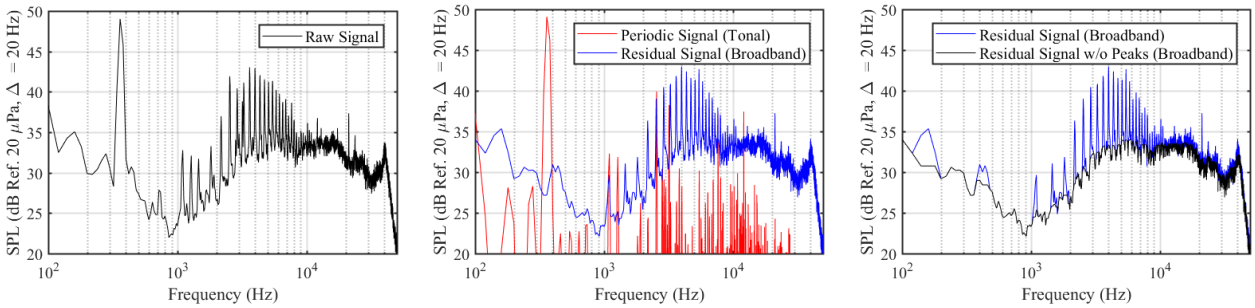

(a) Step 1 (b) Step 2 (c) Step 3

Figure 5. Processing steps for isolation of periodic and broadband noise contributions.

C. Experimental Broadband Noise Trends

1. *Rotational Rate Sweep*

To understand how broadband noise trends with thrust, Figure 1 shows processed broadband noise for all seven rotational cases at $\Theta_T = 6.9°$. To clearly see the differences in thrust conditions, the broadband noise is presented with peaks removed. The high frequency content between $50kHz$ and $60kHz$ present in the lower RPM cases is not a physical mechanism, but the result of limitations in the data acquisition of the microphone signal. Additionally, motor noise located between $21kHz <\approx f <\approx 26kHz$ is present in the data for lower RPM conditions. The noise below about $1kHz$ is believed to be due to disturbances near the microphone.

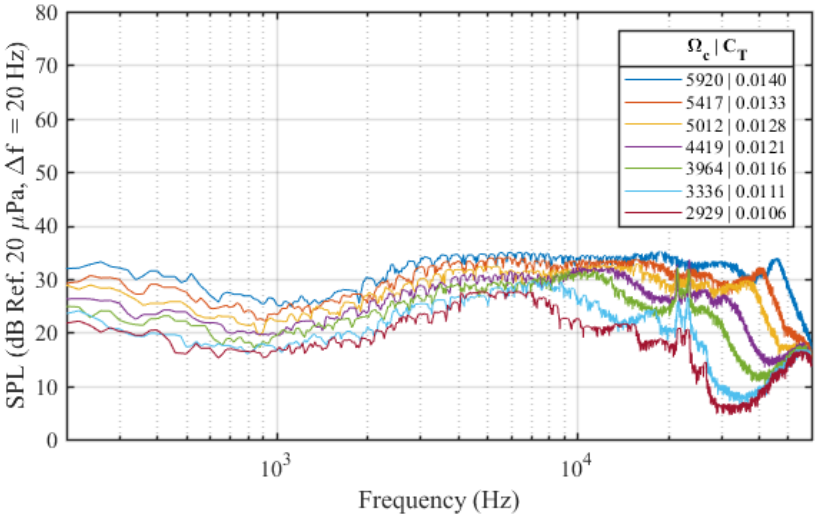

Figure 6. Narrowband Processed Predictions

Some general observations can be made at this point. The highest RPM case has broadband noise spread over a larger range of of frequencies, with the exception of a high frequency "hump" that occurs at around $46kHz$. This noise source is present as you decrease rotational rate, though its presence is diminished. This is characteristic of bluntness-vortex shedding, a self-noise mechanism resulting from vortices forming at the trailing edge and shedding into the airfoil's wake(Ref.,[92]). The noise at the lower rotational rates is less spread out over large frequencies , as can be seen for the 2929 RPM case between $1kHz \leq f \leq 10kHz$. Thus, different noise sources are more prominent with different rotation rates. Lastly, it's interesting to point out that the noise sources, indicating a similar transition between the lower frequency noise sources and higher frequency noise sources is occurring. Thus it could be the case that below 4419 RPM the boundary layer is transitioning differently than at the higher RPMs. To understand this better, the experimental data must

be looked at further with spectral scaling.

Both dimensional and non-dimensional trends of the broadband noise are presented in Figure 7 for the seven RPM cases. The peak-removed broadband spectra for the various thrust conditions are presented as one-third octave spectra ($SPL_{1/3}$) in Figure 7(a). The data was then non-dimensionalized, using the Strouhal number $St = f \star c/U_\infty$ and Tip Mach Number M_{tip}^5 of the highest RPM Case. The scaling was applied and can be seen in Figure 7(b) . This collapses the data along some of the frequencies, but it can be seen that for a Strouhal number range of $0.1 \leq St \leq 0.4$ & $2 \leq St \leq 5$ there is broadband noise that doesn't scale as initially expected. This is believe to be due to the laminar to turbulent boundary layer transition behaviour that is occurring for changing rotor speeds.

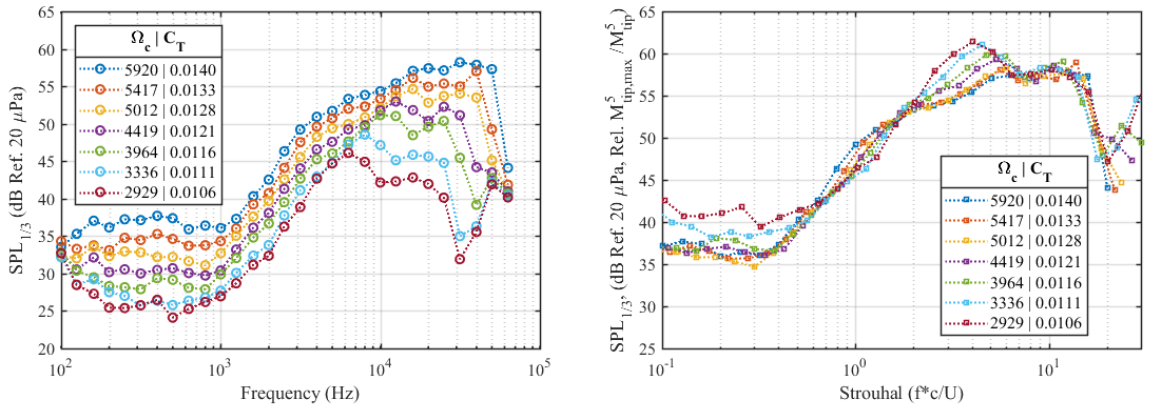

(a) Dimensional Spectra

(b) Non-Dimensional Spectra

Figure 7. Processed broadband spectra for a range of rotation rate conditions.

2. *Pitch Sweep*

Figure 2 shows the spectra for the different blade pitch conditions of $\Theta_T = 4°$, $7°$ and $10°$. A few observations can be made when comparing collective conditions to the baseline case (pictured in red in the figure). First, there is additional broadband noise presents for both collective conditions, between the frequencies of $12kHz <\approx f <\approx 35kHz$. For the lower collective case pictured in blue, this additional noise occurs $20kHz <\approx f <\approx 35kHz$, but for the higher collective case pictured in black, this additional noise occurs at the lower frequencies of $12kHz <\approx f <\approx 23kHz$. The noise peaks at around $16kHz$ and $19kHz$are indicative of laminar bluntness vortex shedding, and it this mechanism is present in both pitch collective cases. However the lower pitch collective the additional noise at the $12kHz <\approx f <\approx 23kHz$ range indicates more pressure side turbulent boundary layer noise. Finally, at the highest frequencies there is bluntness vortex shedding present for all pitch angles, though this mechanism is highest for the $\Theta_{tip} = 9.9°$ case.

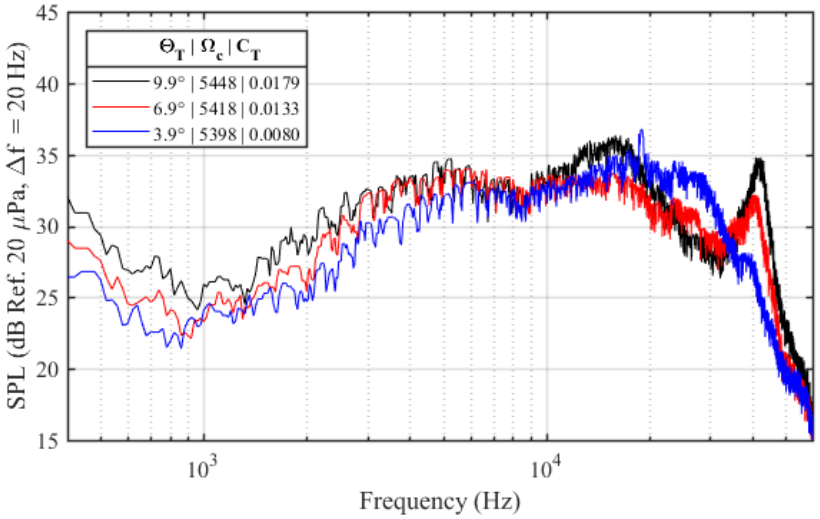

Figure 8. RPM sweep narrowband for microphone 5, for $\Theta_{tip} = 7$ degrees

D. Low Fidelity Predictions

1. *Tonal Noise Predictions*

PAS is used initially to perform a tonal noise prediction of the ideally twisted rotor at the target design operating condition. Figure 9(a) shows the predicted blade passage frequency (BPF) directivity for a range of observer elevation angles (see Fig. 3(c) for angle convention). Note that the data in this figure are normalized to a common radius of 1.90 m using spherical spreading. As Fig. 9(a) shows, the BPF directivity is seen to be thickness noise dominant across the entire range of computed observers. This is because of the relatively large rotor solidity and blade count, which reduces the aerodynamic loading per blade. As a result of this, it is expected that operating the rotor at different collectives for a fixed rotation rate would yield very similar noise levels. This is confirmed in Fig. 9(b), which shows excellent commonality in directivity trends between the PAS predictions and SHAC measurements. The experiments show a maximum difference in levels between the lowest and highest blade pitch settings of 2.5 dB, which is very small compared to the considerable difference in thrust generated by the rotor at the different respective blade pitch settings (see Fig. 4(a)). These results provide further confidence in the low-fidelity blade design and modeling process.

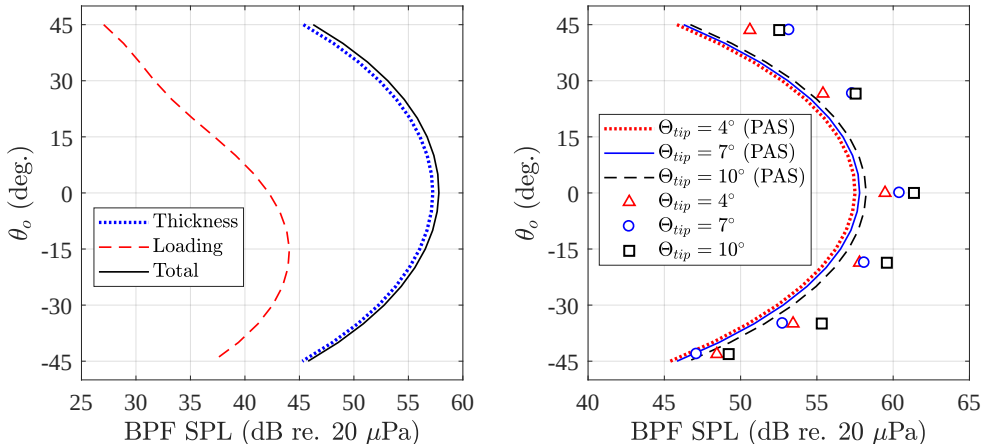

(a) PAS-predicted BPF Directivity

(b) BPF Directivities for Varying Θ_{tip}

Figure 9. Acoustic directivity predictions and measurements of rotor BPF: (a) noise contribution predictions using PAS at target operating condition ($\Theta_{\text{tip}} = 6.9°$), (b) comparison between PAS predictions and experimental SHAC measurements for different blade collective settings.

2. *Broadband Noise Predictions*

As described earlier, low fidelity self-noise predictions have been made using ROTONET and BARC. The self-noise predictions are highly sensitive to the defined boundary layer condition. Figure 10(a) shows a comparison of the experiment baseline case to three different BARC predictions using three different settings. Even though the rotor is physically smooth, an untripped-boundary layer condition does not capture the separation and suction noise that occurs between $1kHz <\approx f <\approx 5kHz$. Broadband noise at this frequency does trend better with a tripped boundary layer condition, but the content between $10kHz$ and is $30kHz$ behaves as laminar bluntness vortex shedding (as shown by the spectral scaling trends of the experiment). So, it was attempted to *partially trip* the last 5% portion of the blade, and the initial physical justification for this decision is that this portion of the blade may be experiencing a tip vortex that is impinging inboard, creating a boundary layer that is more tripped than untripped for a certain distance inboard. It is noted that in Figure 10(a), the 95% *untripped* prediction is over-predicting the LBLVS contribution. In the final paper, additional limiting of the laminar boundary layer mechanism by a parameter such as Reynolds Number will be investigated. Additionally, simulations performed in an accompanying paper which indicate tip vortex spillage acting upon 5% of the blade span further confirms a partial trip condition. Using this partially tripped prediction, it is possible to see the self-noise source broken down in Figure 10(b). This spectra is presented in one-third octave bands to better distinguish the noise sources.

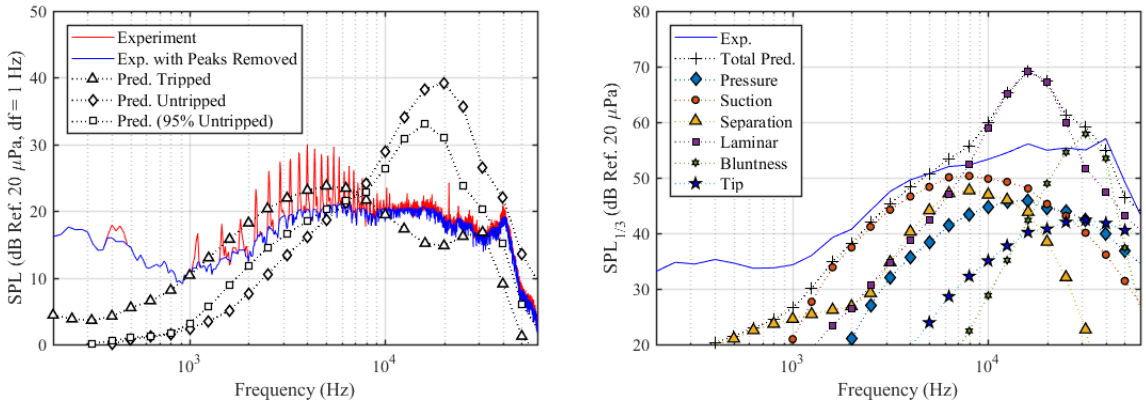

(a) Comparing boundary layer settings to the experiment case.

(b) Self-noise breakdown for the partially tripped (95% untripped) prediction.

Figure 10. Self-noise predictions for the baseline experimental case ($\Theta_{tip} \approx 6.9, \Omega_c \approx 5420$).

III. Plans for Full Paper

The 3-D printed ideally rotor matched performance expectations when tested in the SHAC, and acoustic trends were identified for the rotational sweep and collective conditions.It is believed that laminar bluntness vortex shedding is present for this ideally twisted rotor at all rotational rates, but dominant at the lower tip speeds. By scaling the Strouhal number based on the rotor chord it was possible to see that the laminar boundary layer vortex shedding mechanism is not present at all rpm conditions, however better scaling can be achieved using boundary layer conditions. The experiments have shown that varying collective pitch significantly changes the noise sources and inflow conditions, so additional measurements in the SHAC will be taken to present in the final paper.

Using low fidelity tools, initial predictions are able to reasonably predict the tonal and broadband noise trends of this tested rotor. However, the application of the broadband noise prediction method must be improved for the final paper as the different conditions may have different requirements (for example, limiting the LBL-VS mechanism as it does not seem to be as present for the highest thrust conditions). Additionally,, the boundary layer thicknesses which directly impact the self-noise calculation must be defined properly. A coarse radial grid was used for these predictions to quickly identify trends with different operating conditions, and it is necessary to refine the grid especially near the tip. This is because certain noise mechanisms are very sensitive to the boundary layer conditions that change along the radius. Findings of the

For future $A_\circ \approx \pm 3^\circ$ collective case predictions, it is the intention to employ the use of CAMRAD II to calculate inflow conditions as it is a more comprehensive tool with a free wake model option. It is suspected that additional broadband noise mechanisms may be present at certain operating conditions such as blade wake interaction and turbulence ingestion. The results of an accompanying paper will investigate these noise sources with a lattice-Boltzmann method solver. Also, an experimental flow field survey may provide insight into the non-uniform inflow that is occurring at $A_\circ \approx \pm 3^\circ$ test conditions.

For the final paper, semi-empirical predictions will be presented using the ANOPP2 Self Noise Internal Functional Module (ASNIFM), which can be used with the rest of the ANOPP2 suite to characterize and predict the noise impact of full vehicle designs. This tool will be publicly available and is currently undergoing beta testing.

Acknowledgments

The authors would like to thank the NASA Revolutionary Vertical Lift Technology (RVLT) project and the NASA Langley Center Innovation Fund of Internal Research and Development (CF-IRAD) for funding this work. In addition to this, Siena Whiteside who led the effort of the Aeronautics Systems Analysis Branch in design and printing of the blades used in this experiment. Beau Pollard who designed the 3D blades and Shali Subramanian who aided in both manufacturing and testing the blades in the SHAC. Finally,

the LSAWT team (John Swartzbaugh, Stan Mason, Jeff Collins, Bryan Lamb and Mick Hodgins) who helped with testing in the SHAC.

References

[1]Lopes, L. V. and Burley, C., *ANOPP2 User's Manual: Version 1.2*, Hampton, VA, NASA/TM-2016-219342.

[2]Pettingill, N. A. and Zawodny, N. S., "Identification and Prediction of Broadband Noise for a Small Quadcopter," *VFS Forum 75*, 2019.

[3]Leishman, J. G., *Principles of Helicopter Aerodynamics*, chap. 3.3: Blade Element Momentum Theory (BEMT), Cambridge University Press, 2nd ed., 2002, pp. 87–113.

[4]Whiteside, S. K. S., Zawodny, N. S., Fei, X., Pettingill, N. A., Patterson, M. D., and Rothhaar, P. M., "An Exploration of the Performance and Acoustic Characteristics of UAV-Scale Stacked Rotor Configurations," *AIAA SciTech Forum*, No. January, 2019, pp. 1–20.

[5]Stephenson, J. H., Weitsman, D., and Zawodny, N. S., "Effects of flow recirculation on unmanned aircraft system (UAS) acoustic measurements in closed anechoic chambers," *The Journal of the Acoustical Society of America*, Vol. 145, No. 3, 2019, pp. 1153–1155.

[6]Nguyen, L. C. and Kelly, J. J., *A Users Guide for the NASA ANOPP Propeller Analysis System*, Hampton, VA, 1997, NASA CR 4768.

[7]Weir, S. D., Jumper, J. S., Burley, C. L., and Golub, A. R., "Aircraft Noise Prediction Program Theoretical Manual: Rotorcraft System Noise Prediction System (ROTONET), Part 4," NASA TM 83199, April 1995.

[8]Brooks, T. F., Pope, D. S., and Marcolini, M. A., "Airfoil Self-Noise and Prediction," NASA RP 1218, 1989.

[9]Burley, C. L. and Brooks, T. F., "Rotor Broadband Noise Prediction with Comparison to Model Data," *Journal of the American Helicopter Society*, Vol. 49, No. 1, January 2004, pp. 28–42.

[10]Zawodny, N. S., Boyd Jr., D. D., and Burley, C. L., "Acoustic Characterization and Prediction of Representative, Small-Scale Rotary-Wing Unmanned Aircraft System Components," *72nd American Helicopter Society Annual Forum*, May 2016.

[11]Brooks, T. F., Marcolini, M. A., and Pope, D. S., "Main Rotor Broadband Noise Study in the DNW," *Journal of the American Helicopter Society*, Vol. 34, No. 2, 1989, pp. 3–12.

[12]Zawodny, N. S. and Pettingill, N. A., "Acoustic Wind Tunnel Measurements of a Quadcopter in Hover and Forward Flight Conditions," *47th International Congress and Exposition on Noise Control Engineering*, August 2018.